The final publication is available at

https://doi.org/10.1016/j.saa.2019.117652

Additional Information

Investigation of metabolite-protein interactions by transient absorption spectroscopy and *in silico* methods

Daniel Limones-Herrero,[a] Fabrizio Palumbo,[a] Victoria Vendrell-Criado,[a] Inmaculada Andreu,[b] Emilio Lence,[c] Concepción González-Bello,[c] Miguel A. Miranda[a,b*] and M. Consuelo Jiménez[a,b*]

[a]*Departamento de Química/Instituto de Tecnología Química UPV-CSIC, Universitat Politècnica de València, Camino de Vera s/n, 46022, Valencia, Spain*
[b]*Unidad Mixta de Investigación UPV-Instituto de Investigación Sanitaria (IIS) La Fe, Hospital Universitari i Politècnic La Fe, Avenida de Fernando Abril Martorell 106, 46026, Valencia, Spain*
[c]*Centro Singular de Investigación en Química Biolóxica e Materiais Moleculares (CIQUS), Departamento de Química Orgánica, Universidade de Santiago de Compostela, Jenaro de la Fuente s/n, 15782 Santiago de Compostela, Spain*

ARTICLE INFO

ABSTRACT

Transient absorption spectroscopy in combination with *in silico* methods has been employed to study the interactions between human serum albumin (HSA) and the anti-psychotic agent chlorpromazine (**CPZ**) as well as its two demethylated metabolites (**MCPZ** and **DCPZ**). Thus, solutions containing **CPZ**, **MCPZ** or **DCPZ** and HSA (molar ligand:protein ratios between 1:0 and 1:3) were submitted to laser flash photolysis and the ΔA_{max} value at $\lambda = 470$ nm, corresponding to the triplet excited state, was monitored. In all cases, the protein-bound ligand exhibited higher $\Delta Amax$ values measured after the laser pulse and were also considerably longer-lived than the non-complexed forms. This is in agreement with an enhanced hydrophilicity of the metabolites, due to the replacement of methyl groups with H that led to a lower extent of protein binding. For the three compounds, laser flash photolysis displacement experiments using warfarin or ibuprofen indicated Sudlow site I as the main binding site. Docking and molecular dynamics simulation studies revealed that the binding mode of the two demethylated ligands with HSA would be remarkable different from **CPZ**, specially for **DCPZ**, which appears to come from the different ability of their terminal ammonium groups to stablish hydrogen bonding interactions with the negatively charged residues within the protein pocket (Glu153, Glu292) as well as to allocate the methyl groups in an apolar environment. **DCPZ** would be rotated 180º in relation to **CPZ** locating the aromatic ring away from the Sudlow I of HSA.
.

1. Introduction

Biological interactions between drugs or their metabolites and proteins are of relevance in connection with the knowledge of the cellular activity and with the biochemical paths involved in some medical conditions.[1] Specifically, binding of drugs or their metabolites to transport proteins such as serum albumins (SAs) or α_1-acid glycoproteins (AAGs) determines aspects such as activity, distribution, toxicity or excretion rate of these ligands.[2] Besides, when metabolites are present simultaneously with the parent drugs, it is also relevant to investigate whether this situation results in modification of some aspects of drug behavior.[3]

A number of studies have been devoted to the binding of drugs and metabolites to serum proteins using different approaches. Hence, *in vitro* techniques have been the most employed for this purpose. They include radiometry, surface plasmon resonance, nuclear magnetic resonance and fluorescence spectroscopies, calorimetry, crystallography, equilibrium dialysis, ultrafiltration, ultracentrifugation, chromatography or capillary electrophoresis. In parallel, *in silico* tools allow accurate predictions of the configuration of the protein binding site, by analyzing the thermodynamically most favored configurations. Remarkably, the use of *in vitro* results as a starting point for application of computational tools, results in an optimized characterization of the metabolite-protein interactions and of the nature and structural characteristics of the binding sites.[4]

In this context, the development of tools for investigating metabolite-protein binding remains of great interest. A possibility is the use of a combined methodology that employs laser flash photolysis (LFP) as *in vitro* technique together with docking and molecular dynamics simulation studies as *in silico* tools.

To prove the concept, we selected as metabolites the two demethylated derivatives (**MCPZ** and **DCPZ**) of the anti-psychotic agent chlorpromazine (**CPZ**), a drug employed over decades for the treatment of schizophrenia. [5] Their chemical

structures are shown in Chart 1. Since **MCPZ** and **DCPZ** maintain the **CPZ** chromophore unaltered, any possible modulation of the biological behavior should be correlated with the nature of the aminoalkyl side-chain. In particular, biotransformation could lead to a modified affinity to transport proteins, leading to a different bioavailability.

The absorption spectra of **CPZ** shows the UV–Vis features typical of the phenothiazine chromophore, reaching the UVA zone; in MeCN, the fluorescence maximum is located at $\lambda_{max} =$ 451 nm. [6] The transient absorption spectrum in MeCN displays a maximum at $\lambda_{max} = 470$ nm, attributed to the first triplet excited state, [7] while in PBS, the main maximum appears at $\lambda = 525$ nm, and is ascribed to **CPZ** radical cation (**CPZ$^{\bullet+}$**). [8] The transient absorption spectra of **MCPZ** and **DCPZ** in aqueous medium (PBS, air), display contributions from the radical cation and the triplet excited state. For the parent drug and the two metabolites, the triplet lifetime (τ_T) values, monitored $\lambda = 470$ nm, were lower than 1 µs and increased with the methylation degree. [7b]

CPZ R^1 = R^2 = Me
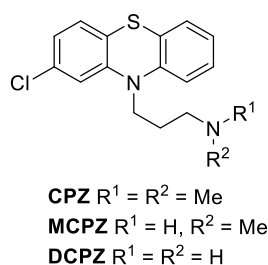**MCPZ** R^1 = H, R^2 = Me
DCPZ R^1 = R^2 = H

Chart 1. Chemical structures of **CPZ**, **MCPZ** and **DCPZ**.

As protein, we selected human serum albumin (HSA) the most abundant transport protein in plasma, responsible for carrying endogenous or exogenous agents in the bloodstream. Binding of drugs and metabolites to HSA can enhance or decrease drug's performance, since the unbound fraction is generally the one that exhibits pharmacological effect and may be metabolized and/or excreted. The human serum albumin (HSA) structure consists of a single chain of 585 amino acids containing only one tryptophan (Trp) residue; the secondary structure is made by 67% of α helix of six turns; the three-dimensional structure is described in terms of three domains, each of them constituted in turn by two subdomains. [9] In general, small organic molecules bind primarily to high-affinity sites, with association constant values in the range of 10^4-10^6 M^{-1}. The pioneering work of Sudlow and coworkers, based on displacement of fluorescence probes, showed that a considerable number of drugs bind with high affinity to site I and site II. [10]

Interaction of **CPZ** with HSA and bovine serum albumin (BSA) has been investigated in the past using equilibrium dialysis, gel filtration or fluorescence quenching. It has been described that binding occurs mainly to one site, with an affinity constant in the range of 10^4-10^5 M^{-1}. [11] However, no information about binding of **CPZ** metabolites is available, although characterization of such metabolite-protein interactions would be very useful for a better understanding of the biochemical pathways involved in various biological conditions. [12] Different methodologies have been employed to investigate binding of metabolites to proteins; they involve either examination of the protein-bound metabolites or determination of the free concentrations of these species. [13] The former approach is of course preferable and provides deeper insight into the nature of the binding process.

The properties of triplet excited states result to be markedly medium-dependent; in this context, they can be excellent reporters to investigate compartmentalized microenvironments, including the protein binding pockets. [14]. We have previously shown that the behavior of triplet excited states of ligands within transport proteins (such as α₁-acid glycoproteins or serum albumins), monitored by transient absorption spectroscopy, constitutes a powerful tool to examine drug binding. [15]
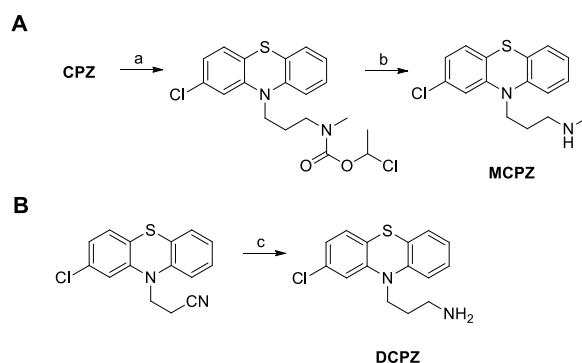
The methodology could also be applied to compare the protein binding behavior of a given drug and its metabolites. Thus, **CPZ** and their demethylated metabolites could be suitable candidates to explore this methodology, given the possibility of generating and monitoring their triplet excited states. Moreover, upon encapsulation, formation triplet excited states could be favored over generation of ionic species (such as radical ions) within the protein binding sites, as previously observed for other ligands. [16] Finally, the protein microenvironment could also protect the encapsulated ligands, resulting in an enhanced photosafety, as described for the HSA binding of cinacalcet; under these conditions, this drug is protected from attack by oxygen and from the phototoxic effects produced by singlet oxygen formation. [15e]

The aim of the present work is to compare binding of **CPZ** and its two demethylated metabolites **MCPZ** and **DCPZ** to HSA by monitoring the triplet excited state of the three compounds by transient absorption spectroscopy. Although the metabolites maintain the same chromophore as parent **CPZ**, they should exhibit an enhanced hydrophilicity due to the replacement of methyl groups with H, leading to a lower extent of protein binding. The obtained results confirm these expectations and are in full agreement with theoretical calculations.

2. Results and Discussion

2.1. Synthesis

The two metabolites **MCPZ** and **DCPZ** were obtained using procedures previously described in the literature. [17] Thus, synthesis of **MCPZ** was carried out in two steps by treatment of **CPZ** with 1-chloroethyl chloroformate followed by reaction with MeOH (Scheme 1A), while **DCPZ** was obtained by reduction of 3-(2-chloro-10H-phenothiazin-10-yl) propanenitrile with LiAlH₄ [18] (Scheme 1B).

Scheme 1. Synthesis of MCPZ (A) and DCPZ (A). *Reagents and conditions*: (a) ethyl formate, DCM, 0 ºC. (b) MeOH, reflux. (c) LiAlH₄, THF, reflux.

2.2. Photophysical Studies

As expected, the absorption spectra of **CPZ**, **MCPZ** and **DCPZ** in PBS were very similar, with maxima at *ca.* 254 y 305 nm (Supplementary Material, Figure S1); in the presence of HSA, a slight bathochromic shift was observed (Figure S2).

The parent drug and the two metabolites displayed a weak fluorescence in PBS, under nitrogen, centered at 453 nm (Figure S3). In all cases, the ϕ_F values were lower than 0.01 (3.6×10^{-3} for CPZ, 4.3×10^{-3} for **MCPZ** and 7.6×10^{-3} for **DCPZ**). In the

presence of HSA (Figure S4), the emission maxima did not shift significantly, but the band was somewhat more intense, (ϕ_F = 6.4 × 10⁻³, 6.9 × 10⁻³ and 8.4 × 10⁻³ for **CPZ**, **MCPZ** and **DCPZ**, respectively).

The triplet excited states of **CPZ**, **MCPZ** and **DCPZ** were then used as reporters for the microenvironments experienced within HSA. Laser flash photolysis of the three compounds was performed at λ_{exc} = 308 nm, in 0.01 M PBS, under aerobic atmosphere. Figures 1A-C show the spectra obtained 0.2 μs after the laser pulse in the presence and absence of HSA. Remarkably, the band peaking at 470 nm, corresponding to the triplet excited state, was much more prominent in the presence of HSA than in aqueous solution, especially in the case of the parent drug.

A complete set of transient spectra for **CPZ**, **MCPZ** and **DCPZ**, both alone and in the presence of HSA, at different delay times are provided in the Supplementary Material (Figure S5). These data are consistent with the coexistence of the triplet excited state (maximum at λ = 470 nm) and the radical cation (maximum at 530 nm) of the drug and its metabolites under all conditions, with the formed species being much longer lived in the presence of protein.
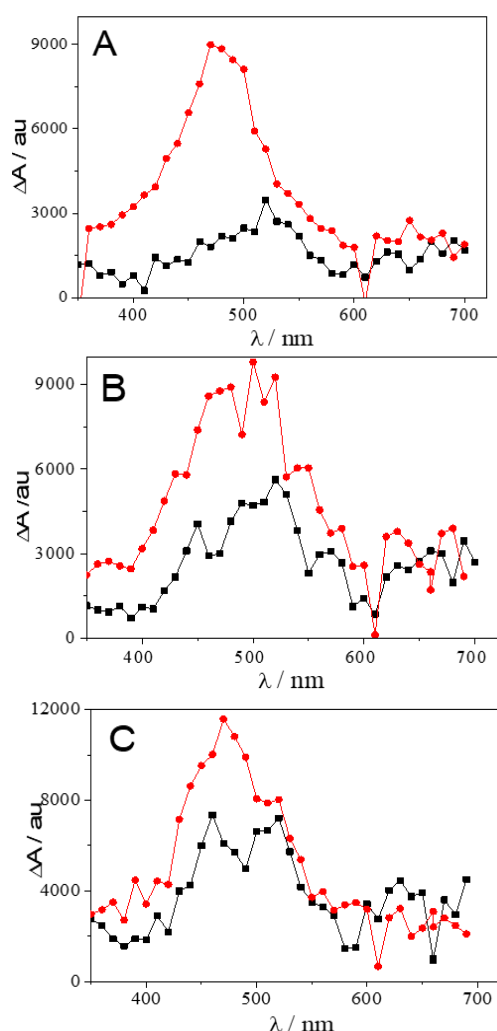

Figure 1. Laser flash photolysis of **CPZ** (A), **MCPZ** (B) and **DCPZ** (C) at λ_{exc} = 308 nm, in PBS, air. Spectra obtained 0.2 μs after the laser pulse in the absence (black trace) or presence (red trace) of 2 equivalents of HSA.

Non-covalent binding was then monitored by following the enhancement of the ΔAmax value at λ = 470 nm in the presence of increasing quantities of HSA. For that purpose, a battery of

PBS solutions containing **CPZ**, **MCPZ** or **DCPZ** and HSA (molar ratios between 1:0 and 1:3) were prepared and monitored by laser flash photolysis. In all cases, the protein-bound ligand decays exhibited higher ΔAmax value and were considerably longer than those of the non-complexed forms (Figures 2A-C, under air); see Figure S6 for the case of **CPZ** under nitrogen. The parent drug **CPZ** exhibited the highest affinity towards HSA, as indicated by the fact that the ³**CPZ*** signal, almost negligible in PBS, clearly increased after addition of only 0.5 equivalents of HSA.
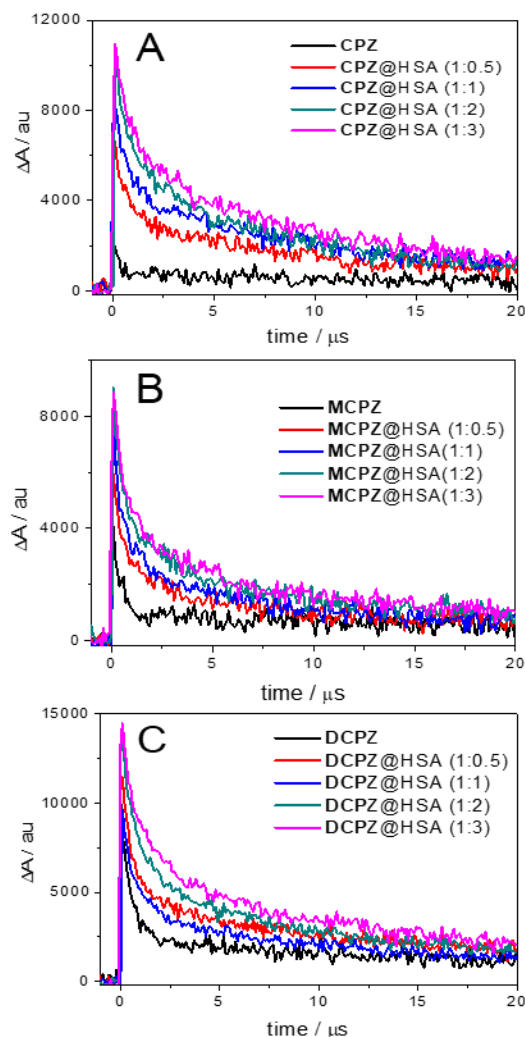

Figure 2. Laser flash photolysis of **CPZ** (A), **MCPZ** (B) and **DCPZ** (C) at λ_{exc} = 308 nm, in PBS, air. Decays monitored at 470 nm in the presence of different amounts of HSA

Then, the binding of **CPZ**, **MCPZ** or **DCPZ** to HSA was compared, using data obtained from transient absorption spectroscopy experiments. Hence, the plot of ΔAmax/ΔA₀ value at λ = 470 nm *vs* HSA concentration showed that the parent drug displays higher affinity for the protein than the two metabolites; this is in agreement with its more lipophilic nature (Figure 3). In the three cases, the binding constants were found to be in the 10⁴-10⁵ range, with **CPZ** > **MCPZ** > **DCPZ** (see Figure S7 for an estimation based on treatment of the ΔAmax/ΔA₀ data). This constitutes a straightforward methodology to determine the relative binding of a drug and its metabolites to a given protein.

Laser flash photolysis measurements were then performed using displacement probes, warfarin (WAR) for site I and

ibuprofen (IBU) for site II, to elucidate the binding site of **CPZ**, **MCPZ** and **DCPZ** within HSA Thus, addition of WAR to a
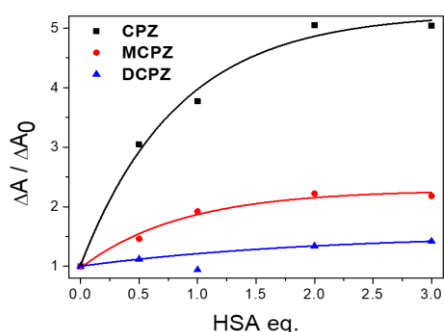

Figure 3. Relative binding of **CPZ**, **MCPZ** or **DCPZ** to HSA, calculated from the ΔA_{max} value at $\lambda = 470$ nm in the presence of increasing amounts of HSA.

CPZ/HSA mixture led to a significant decrease of the ΔA_{max} value at $\lambda = 470$ nm (Figure 4A), indicating displacement of the initially bound drug from the binding site I to the bulk solution. However, addition of IBU to the **CPZ**/HSA mixture did not result in important changes of ΔA_{max} at 470 nm (Figure 4A). A similar trend was observed for **MCPZ** and **DCPZ** (Figures 4B,C). This is consistent with preferential binding of the three investigated compounds to site I.
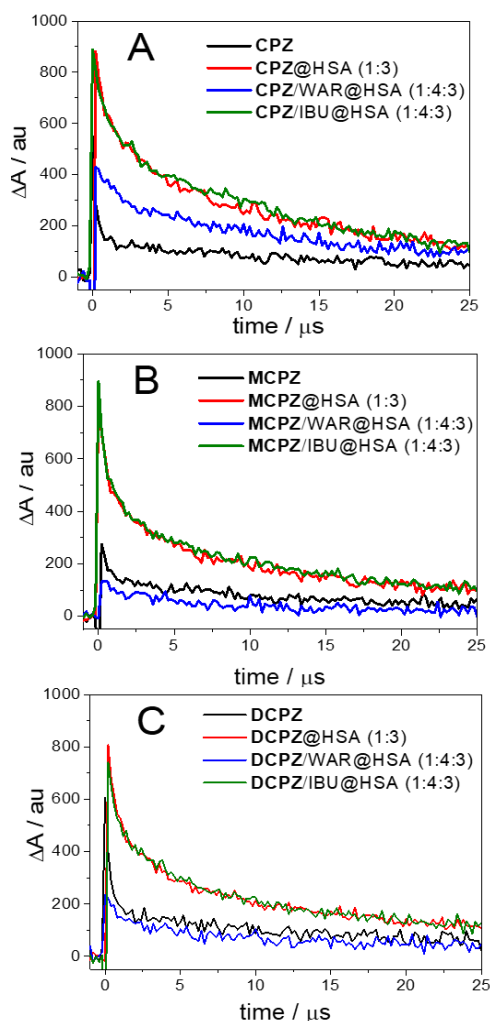

Figure 4. Laser flash photolysis of **CPZ** (A), **MCPZ** (B) and **DCPZ** (C) at $\lambda_{exc} = 308$ nm, in PBS, air. Decays monitored at 470 nm in the presence of site I (WAR) or and site II (IBU) probes. Concentration of ligand was 8×10^{-5} M. Molar ratios are indicated in parenthesis.

2.3. Computational Studies

In an effort to get a better understanding in atomic detail of the differences experimentally obtained in the affinity of **CPZ** and its two metabolites, **MCPZ** and **DCPZ**, to HSA, molecular docking studies were first carried out. These studies were performed using GOLD 5.2.2 [19] program and the protein coordinates found in the crystal structure of HSA in complex with oxyphenbutazone [4-butyl-1-(4-hydroxyphenyl)-2-phenylpyrazolidine-3,5-dione] (PDB entry 2BXB [20]). Among the available crystallographic structures of HSA with a ligand in drug-binding site Sudlow I [10] (sub-domain IIA), the latter was chosen because the arrangement of oxyphenbutazone in 2BXB might be in some extend close to the expected for the tricyclic moiety of **CPZ**. This drug has two benzene rings joined by a central six-membered ring. An analysis of the binding pocket revealed that Sudlow I is a large spherical and amphiphilic pocket located in the vicinity of the sole tryptophan residue in HSA (Trp214). Thus, half of the pocket is mainly lipophilic as it is composed by apolar residues (Leu238, Ala261, Ile264, Ile290, Ala291, Leu260, Leu219, Phe223, etc.) and the second half is polar as it contains mainly four polar residues, specifically Arg257, Tyr150, His242 and Lys199.

Taking into account that the QM/MM (Quantum Mechanics/Molecular Mechanics) calculations reported by Phuangsawai *et al*. [21] revealed that Lys199, His242 and Arg257 are involved in the esterease activity of HSA and that this enzymatic activity involves the neutral Lys199 residue as nucleophile, a neutral protonation state of this residue was considered in these computational studies. Lys199 has an unusually low pK_a of ~8 allowing its chemical modification by compounds such as trifluoromethyl-substituted aryl halides and sulfonates. [22] In addition, as **CPZ** and its two metabolites contain a propylamine chain, which would be protonated at physiological pH, the protonated forms of the ligands were also employed.

On the other hand, taking into account that proteins undergo conformational changes during ligand recognition (induced-fit model) that are not taken into account in docking studies (key-lock model) because the protein is considered as a rigid mold, Molecular Dynamics (MD) simulation studies were subsequently performed with the highest score solution obtained by docking. This type of more complex computational studies: (i) avoids false positives, since the ligands that are not stable in the identified pocket will be expelled from this position; and (ii) provides a more realistic model of the protein/ligand complex. To this end, the GOLD-proposed binding modes of **CPZ** and its two metabolites were further validated by MD simulation studies. These studies were performed for 100 ns by using the monomer of the **CPZ**@HSA, **MCPZ**@HSA and **DCPZ**@HSA protein complexes obtained by docking in a truncated octahedron of water molecules obtained with the molecular mechanics force field AMBER. [23]

2.3.1. Binding Mode of CPZ

Our computational studies showed that **CPZ** would be anchored to Sudlow site I of HSA by a strong hydrogen bonding interaction between the flexible ammonium moiety of the ligand and the carboxylate group of Glu153 (Figure 5). This interaction was observed during about 60% of the simulation with an average value of the distance of 2.9 Å (Figure S8). The arrangement of the aromatic ring in **CPZ** in this sub-pocket would be driven by a strong cation-π interaction between the guanidinium group of Arg257 and the ring containing the chlorine atom.
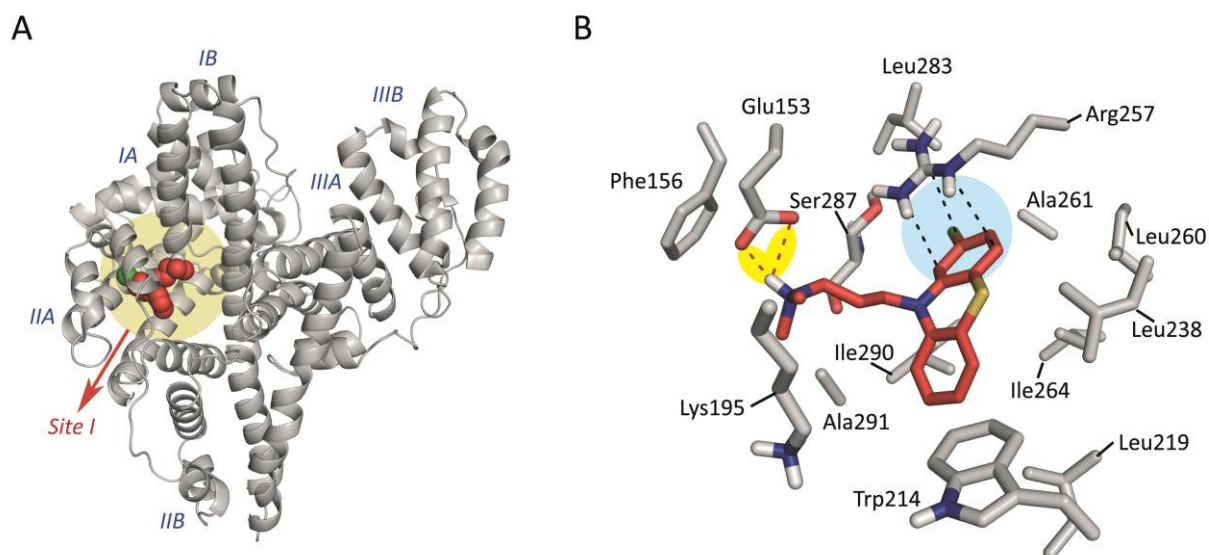
Figure 5. Proposed Binding mode of **CPZ**. (A) Overall view of the **CPZ**@HSA complex obtained by MD simulation studies. Snapshot after 40 ns is shown. The main backbone of **CPZ** is shown as red spheres. The domains I−III and sub-domains (A,B) in HSA protein are labelled. The localization of the ligand in site I is highlighted with a pale yellow background. (B) Relevant interactions of **CPZ** with sub-domain IIA (site I) of HSA. Hydrogen bonding and cation-π interactions between the ligand and the protein are shown as red and black dashed lines and highlighted with a yellow and blue background, respectively. Relevant side chain residues are shown and labelled.
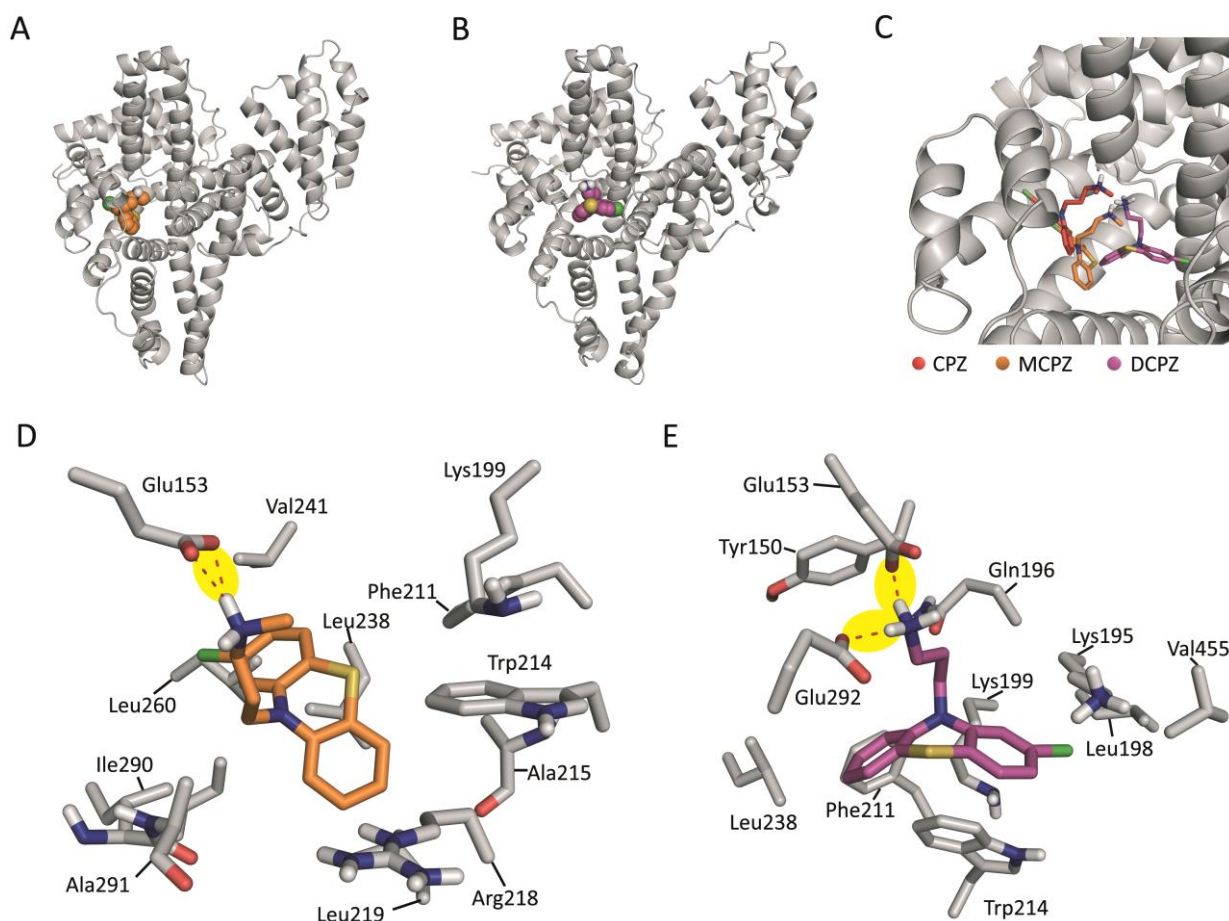

Figure 6. Proposed Binding mode of **MCPZ** and **DCPZ**. (A−B) Overall views of the **MCPZ**@HSA (A) and **DCPZ**@HSA (B) complexes obtained by MD simulation studies. Snapshots after 90 ns and 80 ns, respectively, are shown. The main backbone of MCPZ and DCPZ are shown as orange and purple spheres, respectively. (C) Comparison of the binding mode of CPZ, MCPZ and DCPZ. Note how the binding mode of **DCPZ** is significantly different from **CPZ** and **MCPZ**. (D−E) Relevant interactions of **MCPZ** (D) and **DCPZ** (E) with HSA. Hydrogen bonding interactions between the ligands and the protein are shown as red dashed lines and highlighted with a yellow background. Relevant side chain residues are shown and labelled.

In addition, the aromatic moiety of the ligand would establish numerous favorable lipophilic interactions with the side chain of residues Leu238, Ala261, Ile264, Leu283, Ile290, Ala291, Leu260, Leu219, and Trp214. Both methyl groups in CPZ would

interact with the side chain of Ala291 (strong) as well as the carbon side chain of Lys195 (weaker). Therefore, the position of the ammonium group would be fixed on one face by hydrogen bonding with Glu153 and on the other face with lipophilic interactions with Lys195 (carbon chain) and Ala91.

2.3.2. Binding Mode of the Two Metabolites

The computational studies performed with the two demethylated ligands, **MCPZ** and **DCPZ**, revealed that the binding mode of these ligands with HSA would be remarkable different from the aforementioned for **CPZ** (Figures 6A−C). As expected, the keys of the distinct arrangement of **CPZ** in relation to **MCPZ** and **DCPZ** appears to come from the different ability of their terminal ammonium groups ($-NH^+Me_2$, $-NH_2^+Me$, $-NH_3^+$, respectively) to establish hydrogen bonding interactions with the negatively charged residues within the protein pocket, as well as to allocate the methyl groups in an apolar environment. Thus, for **MCPZ**, the interaction of the methyl group with the side chain of Ala291, which was present in **CPZ**, would be lost. As a result, **MCPZ** would bind to HSA by locating its aromatic ring at the entrance of Sudlow site I but without being able to immerse this moiety in this pocket as for **CPZ** (Figure 6D). As for **CPZ**, the main polar interaction would be between the ammonium group and the carboxylate group of Glu153. This hydrogen bonding interaction was observed during about 67% of the simulation with an average value of the distance of 2.9 Å (Figure S9).

Moreover, **DCPZ** would be rotated 180º in relation to **CPZ** locating the aromatic ring away from the Sudlow site I of HSA and sole tryptophan residue in HSA (Trp214). The driving force of this ligand rotation appears to be the formation of two strong hydrogen bonds, instead of one as in **CPZ** and **MCPZ**, between its ammonium group ($-NH_3^+$) and the carboxylate groups of residues Glu153 and Glu292 (Figure 6E). on top of the These hydrogen bonding interactions were identified during about 84% and 90%, respectively, of the simulation with average values of 2.9 Å for both cases (Figure S10). Moreover, our docking studies revealed that **CPZ** would have the highest binding affinity (scoring) of the three ligands and DCPZ the lowest one. Thus, the ranking affinity would be **CPZ** > **MCPZ** > **DCPZ**, which is in agreement with the experimental results.

As regards the lack of radical cation formation inside HSA, as evidenced by the laser flash photolysis results, computational studies suggest that it would be caused by an increase in the planarity of the tricyclic ring as well as the methylene group directly connected to it. Thus, Joshi *et al.* [5c] reported that the calculated butterfly angle increases from 145.4º in **CPZ** to 157.4º in **CPZ•+**. The larger planarity of the aromatic ring and the subsequent conformational changes in the flexible chain would prevent a deep anchoring of this ring into the apolar sub-pocket as it occurs with **CPZ** (Figure 7).

3. Conclusions

Thus, it can be concluded that transient absorption spectroscopy in combination with docking and molecular dynamics simulation studies constitutes a powerful tool to study binding of drug metabolites to transport proteins. The triplet state decay is a sensitive indicator that clearly discriminates between the free and protein-bound species. In addition, the lipophilic microenvironment existing in the protein cavities favors triplet formation over generation of ionic species such as radical cations. Docking and Molecular Dynamics simulation studies revealed that the binding mode of the two demethylated ligands within HSA would be remarkable different from that of **CPZ**, specially for **DCPZ**, which appears to come from the different

ability of their terminal ammonium groups to stablish hydrogen bonding interactions with the negatively charged residues within the protein pocket (Glu153, Glu292) as well as to allocate the methyl groups in an apolar environment. **DCPZ** would be rotated 180º in relation to CPZ locating the aromatic ring away from the Sudlow I of HSA.
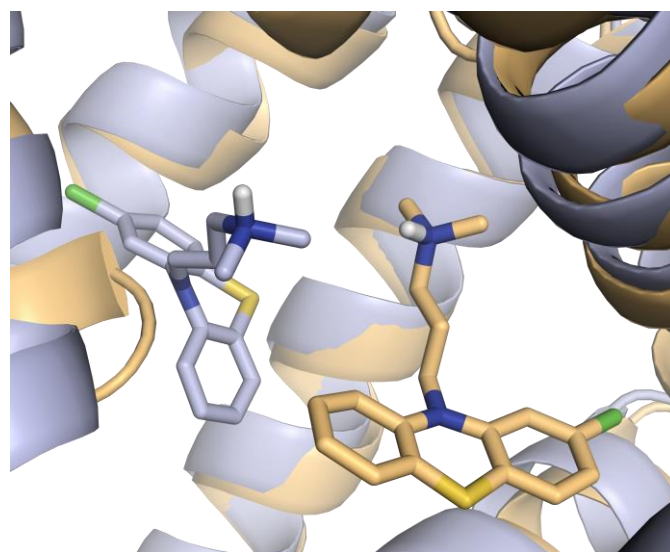

Figure 7. Comparison of the binding mode of **CPZ** (blue) and **CPZ•+** (light orange) with HSA predicted by MD simulation studies. Snapshots after 40 ns and 90 ns, respectively, are shown. Note how the increased planarity of the tricyclic ring in **CPZ•+** would prevent the interaction of aromatic ring with the deep apolar pocket of sub-domain IIA (site I).

4. Experimental Section

4.1. General

Chlorpromazine hydrochloride (**CPZ·HCl**), 3-(2-chloro-10H-phenothiazin-10-yl)propananitrile, 1-chloroethyl chloroformate (ACE-Cl), human serum albumin (HSA), guanidium chloride (GndCl), lithium aluminium hydride (LiAlH₄), warfarin (WAR) and ibuprofen (IBU) were commercially available. Solvents (methanol, 2-butanone, tetrahydrofuran, chloroform) and hydrochloric acid were analytical grade. Phosphate buffer saline solutions (PBS, 0.01 M, pH = 7.4) were obtained by dissolving commercially available phosphate-buffered saline tablets in deionized water. NMR spectra were recorded on a Bruker AV 400 spectrometer at 296K. Chemical shifts are referenced to tetramethylsilane (δ = 0 ppm). HRMS were obtained by electrospray mass spectroscopy in the positive mode using a Xevo QTof MS apparatus (Waters).

4.2. Synthesis of the Metabolites

4.2.1. Synthesis of **MCPZ** [17]

To a well stirred solution of **CPZ** in methylene chloride at 0ºC, ACE-Cl (0.720 ml, 6.7 mmol) was slowly added. Then, the reaction mixture was maintained under reflux for 1h. The solvent was evaporated, the solid was dissolved in diethyl ether (50 mL) and washed with water. The organic layer was dried (MgSO₄), filtered and the solvent removed. The intermediate 3-(2-chloro-10H-phenothiazine-10-yl) was used without further purification. It was then dissolved in methanol and maintained under reflux for 45 min. The solvent was evaporated and **MCPZ** was obtained by crystallization with 2-butanone, in 88% yield. ¹H-RMN (400

MHz, CD$_3$OD), δ (ppm): 7.22 – 7.29 (m, 1H), 7.19 (dd, J_1 = 7.7 Hz, J_2 = 1.4 Hz, 1H), 7.14 (d, J = 8.2 Hz, 1H), 7.04 – 7.10 (m, 2H), 7.01 (ddd, J_1 = 10.2 Hz, J_2 = 7.8 Hz, J_3 = 1.5 Hz, 2H), 4.08 (t, J = 6.4 Hz, 2H), 3.09 (dd, J_1 = 9.1 Hz, J_2 = 6.9 Hz, 2H), 2.63 (s, 3H), 2.15 (tt, J_1 = 12.7, J_2 = 6.4 Hz, 2H); ^{13}C-RMN (100 MHz, CD3OD) (δ, ppm): 148.0, 145.7, 134.7, 129.3, 129.0, 128.7, 127.1, 126.2, 124.7, 124.0, 117.6, 117.4, 48.2, 45.1, 33.7, 24.7; HRMS calcd. for C$_{16}$H$_{17}$N$_2$SCl: 304.0801 [M-HCl], found 304.07881.

4.2.1. Synthesis of *DCPZ* [18]

3-(2-chloro-10H-phenothiazin-10-yl)propanonitrile (200 mg, 0.70 mmol) was placed in a soxhlet and extracted with THF containing LiAlH$_4$ (61 mg, 1.61 mmol). The reaction was stopped adding 5 mL of 20% NaOH aqueous solution. Inorganic salts were removed by filtration and the solvent was extracted with THF. The organic layer was dried over MgSO$_4$. After addition of some drops of HCl, the solvent was evaporated. The hydrochloride salt of **DCPZ** was obtained by crystallization with ethanol, with 35%. ^{1}H-RMN (300 MHz, CD$_3$OD), δ (ppm): 7.25 (ddd, J_1 = 8.2 Hz, J_2 = 7.3 Hz, J_3 = 1.5 Hz, 1H), 7.18 (dd, J_1 = 7.7, J_2 = 1.5 Hz, 1H), 7.13 (d, J = 8.2 Hz, 1H), 7.04 – 7.10 (m, 2H), 6.95 – 7.04 (m, 2H), 4.08 (t, J = 6.4 Hz, 2H), 2.98 – 3.09 (m, 2H), 2.13 (dq, J_1 = 14.2, J_2 = 6.3 Hz, 2H); ^{13}C-RMN (75 MHz, CDCl$_3$) (δ, ppm): 148.0, 145.7, 134.7, 129.3, 128.92, 128.6, 127.0, 126.1, 124.6, 123.9, 117.6, 117.4, 45.2, 38.6, 26.0.

4.3. Fluorescence Experiments

Emission spectra were recorded using a JASCO FP-8500 spectrofluorometer system, provided with a monochromator in the wavelength range 200–850 nm. Fluorescence of the samples was registered after adjusting their absorbance below to 0.2 at the excitation wavelength (λ$_{exc}$= 330 nm). The quartz cells employed were 1 cm path length and 4 mL of capacity. Measurements were performed at room temperature.

4.4. Laser Flash Photolysis Experiments

Laser flash photolysis (LFP) measurements were performed using a pulsed Xe/HCl excimer laser (λ$_{exc}$= 308 nm, 30 mJ per pulse). A pulsed Xe lamp was employed as detecting light source. The LFP device consisted of a pulsed laser, a Xe lamp, a monochromator and a photomultiplier. The output signal from the oscilloscope was transferred to a personal computer. Kinetic traces were monitored at λ = 470 nm. Absorbance of the samples was kept below 0.3 at the excitation wavelength. The quartz cells employed were 1 cm path length and 4 mL of capacity. Measurements were performed at room temperature.

4.5. Docking Studies

They have been performed using GOLD 5.2.2 program [19] and the protein coordinates from the crystal structure of HSA in complex with oxyphenbutazone [4-butyl-1-(4-hydroxyphenyl)-2-phenylpyrazolidine-3,5-dione] (PDB entry 2BXB [20]). The experimental procedure used was similar to that described in [21] for ligand 4-(4-trifluorometylphenyl)phenol.

4.6. Molecular Dynamics Simulations Studies

The ligand minimization (**CPZ**, **MCPZ** and **DCPZ**), the generation and minimization of **CPZ**@HSA, **MCPZ**@HSA and **DCPZ**@HSA binary complexes and MD simulation of the resulting minimized complexes (100 ns) were carried following the protocol described in [21] for ligand 4-(4-trifluorometylphenyl)phenol. The ligand/protein structures herein disclosed have been created using the molecular graphics program PyMOL.[22] For the analysis of the trajectories and the rmsd of the protein during the simulation calculated the cpptraj module in AMBER 16 was employed.[23].

Acknowledgments

Appendix A. Supplementary Material

Absorption and fluorescence spectra of **CPZ**, **MCPZ** and **DCPZ** in the absence and presence of HSA; laser flash photolysis of spectra od **CPZ**, **MCPZ** and **DCPZ** at different delay times in the absence or presence of HSA, modified Benessi-Hildebrand plots and variation of the relative distances for selected atoms in ligand@protein complexes.

References

1. G.X. Yang, X. Li, M. Sinder, Investigating metabolite-protein interactions: an overview of available techniques, Methods 57(2012), 459-466.
2. D.S. Hage, J. Anguizola, O. Barnaby, A. Jackson, M.L. Yoo, E. Papastravos, E. Pfaunmiller, M. Sobansky, Z. Tong, Characterization of drug interactions with serum proteins by using high-performance affinity chromatography, Curr. Drug Metab. 12(2011), 313-328.
3. R. Matsuda, C. Bi, J. Anguizola, M. Sobansky, E. Rodriguez, J. Vargas Badilla, X. Zheng, B. Hage, D.S. Hage, Studies of metabolite-protein interaction: a review, J. Chromatogr. B Analyt Technol Biomed Life Sci 966(2014), 48-58.
4. G.X. Yang, X. Li, M. Snyder, Investigating metabolite-protein interactions: an overview of available techniques, Methods 57(2012), 459-466.
5. (a) F. López-Muñoz, C. Alamo, E. Cuenca, W.W. Shen, P. Clervoy, G. Rubio, History of the discovery and clinical introduction of chlorpromazine, Ann. Clin. Psychiatry 17 (2005), 113–135;
   (b) A.H. Beckett, M.A. Beaven, A.E. Robinson, Metabolism of chlorpromazine in humans, Biochem. Pharmacol. 12 (1963) 779–794;
   (c) M. Chetty, S.V. Moodley, R. Miller, Important metabolites to measure in pharmacodynamics studies of chlorpromazine, Ther. Drug Monit. 16 (1994) 30–36;
   (d) J.W. Hubbard, K.K. Midha, E.M. Hawes, G. McKay, S.R. Marder, M. Aravagiri, E.D. Korchinski, Metabolism of phenothiazine and butyrophenone antipsychotic drugs: a review of some recent research findings and clinical implications, Br. J. Psychiatry 163 (1993) 19−24;
6. C. García, R. Oyola, L.E. Piñero, R. Arce, J. Silva, V. Sánchez, Substitution and solvent effects on the photophysical properties of several series of 10-alkylated phenothiazine derivatives, J. Phys. Chem. A 109 (2005) 3360−3371.
7. (a) S. Navaratnam, B.J. Parsons, G.O. Phyllips, A.K. Davies, Laser flash photolysis study of the photoionization of chlorpromazine and promazine in solution, J Chem Soc, Faraday Trans. 1 74 (1978) 1811−1819;
   (b) F. Palumbo, G. Garcia-Lainez, D. Limones-Herrero, M.D. Coloma, J. Escobar, M.C. Jiménez, M.A. Miranda, I. Andreu, Enhanced photo(geno)toxicity of demethylated chlorpromazine metabolites, Toxicol. Appl. Pharmacol. 313 (2016) 131−137.

8. (a) C.C. García, G.A. Smith, W.G. McGimpsy, I.E. Kochevar, R.W. Redmond, Mechanism and solvent dependence for photoionization of promazine and chlorpromazine, J. Am. Chem. Soc. 117 (1995) 10871−10878;
    (b) S. Nath and A.V. Sapre, Photoinduced electron transfer from chlorpromazine and promethazine to chloralkanes accompanied by cleavage of C-Cl bond, Chem. Phys. Lett. 344 (2001) 138−146;
    (c) R. Joshi, T.K. Ghanty, and T. Mukherjee, Reactions and structural investigation of chlorpromazine radical cation, J. Mol. Struct. 888 (2008) 401−408.

9. (a) D.C. Carter, J. X. Ho, Structure of serum albumin, in: V. N. Schumaker (Ed.), Advances in Protein Chemistry, vol 45, Academic Press, New York, 1994, pp 153−203;
    (b) T. Peters (1995) All about Albumins: Biochemistry, Genetics and Medical Applications, Academic Press, San Diego.
    (c) X.M. He, D.C. Carter Atomic structure and chemistry of human serum albumin, Nature 358 (1992) 209−215.

10. G. Sudlow, D.J. Birkett, D. N. Wade, The characterization of two specific drug binding sites on human serum albumin, Mol. Pharmacol. 11 (1975) 824–832.

11. (a) D.J. Sharples, The binding of chlorpromazine to human serum albumin, Pharm. Pharmacol 26 (1974) 640−641;
    (b) R.K. Verbeeck, J. A. Cardinal, A. G. Hill, K. K. Midha, Binding of phenothiazine neuroleptics to plasma proteins, Biochem. Pharmacol. 32 (1983) 2565–2570;
    (c) D. Silva, C.M. Cortez, S.R. Louro, Quenching of the intrinsic fluorescence of bobine serum albumin by chlorpromazine and hemin, Braz. J. Med. Biol. Res. 37 (2004) 963–968;
    (d) E. Lazaro, P.J. Lowe, X. Briand, B. Faller, New approach to measure protein binding based on a parallel artificial membrane assay and human serum albumin, J. Med. Chem. 51(2008) 2009–2017.

12. (a) R. Kaddurah-Daouk, B.S. Kristal, R.M. Weinshilboum, Metabolomics: A global biochemical approach to drug response and disease, Annu. Rev. Pharmacol. Toxicol. 48 (2008) 653–83;
    (b) P. Korkuć and D. Walther, Physicochemical characteristics of structurally determined metabolite-protein and drug-protein binding events with respect of binding specificity, Front. Mol. Biosci. 2 (2015) 1–20.

13. (a) C.M. Ohnmacht, S. Chen, Z. Tong, D. S. Hage, Studies by biointeraction chromatography of binding by phenytoin metabolites to human serum albumin, J. Chromatogr. B 836 (2006) 83–91;
    (b) K.G. Roelofs, J. Wang, H.O. Sintim, V.T. Lee Differential radial capillary action of ligant assay for high-throughput detection of protein-metabolite interactions, Proc. Natl. Acad. Sci. 108 (2011) 15528–15533;
    (c) G.X. Yang, X. Li, M. Synder, Investigating metabolite–protein interactions: an overview of available techniques, Methods 57 (2012) 459–466

14. M.C. Jiménez, M.A. Miranda, Triplet excited states as a source of relevant (bio)chemical information, Curr. Top. Med. Chem. 14 (2014) 2734–2742.

15. (a) M.C. Jiménez, M.A. Miranda, I. Vayá, Triplet excited states as chiral reporters for the binding of drugs to transport proteins, J. Am. Chem. Soc. 127 (2005) 10134–10135;
    (b) I. Vayá, C.J .Bueno, M.C. Jiménez, M.A. Miranda, Use of triplet excited states for the study of drug binding to human and bovine serum albumins, ChemMedChem 1 (2006) 1015–1020;
    (c) I. Vayá, M.C. Jiménez, M.A. Miranda, Transient absorption spectroscopy for determining multiple site occupancy in drug-protein conjugates. A comparison between human and bovine serum albumins using flurbiprofen methyl ester as a probe, J. Phys. Chem. B 112 (2008) 2694–2699;
    (d) R. Perez-Ruiz, C.J. Bueno, M.C. Jiménez, M.A. Miranda, In situ transient absorption spectroscopy to assess competition between serum albumin and alpha-1-acid glycoprotein for drug transport, J. Phys. Chem. Lett. 1 (2010) 829–833;
    (e) E. Nuin, M.C. Jiménez, G. Sastre, I. Andreu, M.A. Miranda, Drug–drug interactions within protein cavities probed by triplet–triplet energy transfer, J. Phys. Chem. Lett. 4 (2013) 1603–1607.

16. (a) R. Alonso, M. Yamaji, M.C. Jiménez, M.A. Miranda, Enhanced photostability of the anthracene chromophore in aqueous medium upon protein encapsulation, J. Phys. Chem. B, 114 (2010) 11363–11369;
    (b) R. Alonso, M.C. Jiménez, M.A. Miranda, Stereodifferentiation in the compartmentalized photooxidation of a protein-bound anthracene, Org. Lett. 13 (2011) 3860–3863;
    (c) D. Limones-Herrero, R. Pérez-Ruiz, M.C. Jiménez, M.A. Miranda, Retarded photooxidation of cyamemazine in biomimetic microenvironments, Photochem. Photobiol. 90 (2014) 1012–1016.

17. K. Kitamura, T. Fujitani, K. Takahashi, Y. Tanaka, S. Hirako, C. Kotani, T. Hashimoto, S. Takegami, Synthesis of [N-^{13}CH$_3$] drugs (chlorpromazine, triflupromazine and promazine), J. Labelled Compd. Radiopharm. 43 (2000) 865–872.

18. Z. Zhou, A.W. Franz, S. Bay, B. Sarkar, A. Seifert, P. Yang, A. Wagener, S. Ernst, M. Pagels, T.J.J. Müller, W. Thiel. Redox active mesoporous hybrid materials by in situ syntheses with urea-linked triethoxysilylated phenothiazines, Asian J. Org. Chem. 5 (2010) 2001–2015.

19. http://www.ccdc.cam.ac.uk/solutions/csd-discovery/components/gold/ (accessed May 1, 2019).

20. J. Ghuman, P.A. Zunszain; I. Petitpas, A.A. Bhattacharya, M. Otagiri, S. Curry, Structural basis of the drug-binding specificity of human serum albumin, J. Mol. Biol. 353 (2005) 38–52.

21. R. Pérez-Ruiz, Ó. Molins-Molina, E. Lence, C. González-Bello, M.A. Miranda, M.C. Jiménez. Photogeneration of quinone-methides as latent electrophiles for lysine-targeting, J. Org. Chem. 83 (2018), 13019−13029.

22. W.L. DeLano, The PyMOL Molecular Graphics System. (2008) DeLano Scientific LLC, Palo Alto, CA, USA. http://www.pymol.org/

23. D.R. Roe, T.E. Cheatham, PTRAJ and CPPTRAJ: software for processing and analysis of molecular and trajectory data, J. Chem. Theory Comput. 9 (2013) 3084–3095.

∗ Corresponding author. Tel.: +0-34-963877800; fax: +0-34-963877809; e-mail: mcjimene@qim.upv.es